

Solar image restoration

M. G. Löfdahl^{1,*}, M. J. van Noort¹, and C. Denker^{2,3}

¹Institute for Solar Physics of the Royal Swedish Academy of Sciences
AlbaNova University Center, Stockholm, Sweden

²New Jersey Institute of Technology, Newark, NJ, U.S.A.

³Astrophysikalisches Institut Potsdam, Potsdam, Germany

**Email:* mats@astro.su.se

Abstract. Image restoration is used to repair solar images degraded by the turbulence in Earth's atmosphere. Restoration algorithms are based on models of the optical system that produce the images – from the solar source of radiation, through Earth's atmosphere and telescope/instrument optics, to the detectors recording the data. In this review, these model components are discussed in the context of two very different classes of image restoration methods, i.e., Speckle Imaging and Phase Diversity/Multi-Frame Blind Deconvolution, which have been successfully used during the last two decades. The strengths and weaknesses of these two approaches are discussed, as well as some variants and recent progress.

1 Introduction

Atmospheric turbulence is the primary obstacle in achieving diffraction-limited resolution in modern ground-based solar observations, as it randomly distorts the wavefronts emanating from the Sun. The results are image motion, blurring, and geometrical distortions of the collected images. Adaptive optics (AO) significantly reduces low-order aberrations but residuals still remain significant. Image restoration techniques can correct higher-order aberrations because they do not suffer from the constraints involved in the AO control system. The most commonly used methods for solar image restoration are Speckle Imaging (SI) and different variants of Multi-Frame Blind Deconvolution (MFBD) and Phase Diversity (PD).

In this review, we present a data collection model for solar imaging, including seeing effects, and state the problem of image restoration in more detail. We describe, with a minimum of mathematics, the two methods including some variants that answer challenges posed by new observing methods and instruments.

2 Data collection model

Understanding the image formation process is necessary for algorithm developers. It is also instructive for interpreters of restored solar data, who want to understand the limitations of image restoration and what improvements are to be expected. Figure 1 illustrates a data collection model suitable for SI and MFBD methods.

The solar image, formed on a detector, is a blurred version of the object. The detector adds random and fixed pattern noise to this blurred image.

In an image processing sense, the object is the solar scene as viewed in a certain wavelength passband and polarization state selected by the filters. Spectral lines are formed at altitudes that vary with wavelength (e.g., line core vs. wing), which results in co-spatial objects with different appearance. The $H\alpha$ image in Fig. 2 shows the chromosphere above a small sunspot. The inset continuum image demonstrates the multi-faceted appearance of structures in different wavelengths.

The algorithms are based on the assumption that blurring can be described as the convolution of an image with a space invariant point spread function (PSF). Therefore, the processing has to be restricted to small subfields, the approximate size of an isoplanatic patch. In the Fourier domain, the convolution with a PSF is equivalent to multiplication with an optical transfer function (OTF). The modulus of the OTF, called the modulation transfer function (MTF), measures the gain as a function of spatial frequency.

The OTF can be formulated as the autocorrelation of the pupil transmission function, which represents the entire optical system including the atmosphere as well as the actual optics. The amplitude of this complex function encodes the size and shape of the pupil and determines the diffraction-limited resolution of the telescope. The phase encodes the optical aberrations, which are the source of the solar image restoration problem. A tilt in the phase moves the image and a phase curvature lowers the MTF at high spatial frequencies and scrambles the Fourier phases of the image. Together, these effects blur the observed image and introduce false structures. A fixed or slowly varying component is related to imperfections in the telescope, re-imaging optics, and filters. However, the difficulties in restoring solar images arise from rapid, random refraction effects in the Earth's atmosphere. They can be partly compensated by AO systems, which have been operational for several years at the major high-resolution solar telescopes (see, e.g., Rimmele 2000; Scharmer et al. 2000; or Berkefeld 2007 and references therein). In addition, a minor, often ignored contribution to the MTF comes from the detector (see, e.g., Stevens & Lavine 1994).

A wavefront emanating from the Sun expands undisturbed through empty space until it enters the Earth's turbulent atmosphere as a plane parallel wave. The atmospheric turbulence is powered by the day–night cycle, which heats and cools the Earth's surface, creating large-scale atmospheric motions. Once these motions become turbulent, large-scale eddies break up, leading to temperature fluctuations across a wide range of spatial scales. The refractive index of air is temperature sensitive so that the fluctuations act as optical elements in front of the telescope aperture. The energy transfer from large- to small-scale turbulent eddies is governed by Kolmogorov's model of atmospheric turbulence (see, e.g., Roddier 1981).

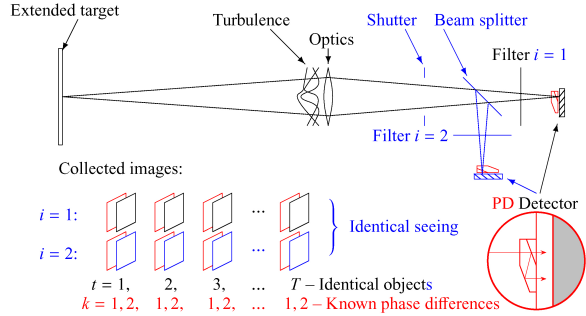


Figure 1. Multiple-object data collection model for SI and MFBD with PD. The two stacks of image frames at the bottom left represent data collected through different filters with index i . Frames collected at a particular time t share the same seeing and k denotes different PD focus positions.

Fried (1966) introduced the parameter r_0 , which is used to characterize the magnitude of atmospheric seeing. The spatial RMS of the wavefront phase over the telescope pupil, $(D/r_0)^{5/6}$, increases almost linearly with D , where D is the diameter of the telescope aperture. The usual interpretation of r_0 has its roots in this expression: the RMS wavefront is 1 rad or $\sim 1/6$ wave over a telescope diameter that equals r_0 . Seeing originating beyond a few hundred meters from the telescope aperture causes anisoplanatic seeing, which varies across field-of-views (FOVs) typically encountered in high-resolution solar physics ($\sim 40''$ to $100''$). Long exposures average over many different atmospheric states and cause a loss of resolution that cannot be undone. However, short-exposure images retain diffraction-limited information by “freezing” the wavefront aberrations (Labeyrie 1970).

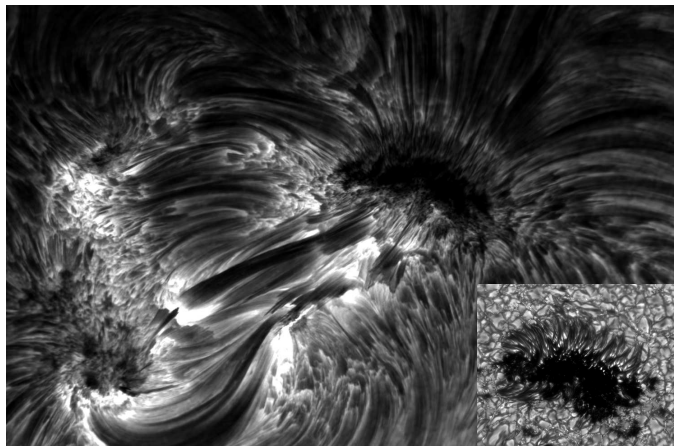


Figure 2. $H\alpha$ image with blue continuum inset demonstrating the appearance of a sunspot at different wavelengths. (MFBD-restored SST images, courtesy of O. Engvold and L. Rouppe van der Voort.)

3 Methods

3.1 Speckle imaging

In SI, the complex Fourier transform of the object is reconstructed from separate estimates of the amplitude (Labeyrie 1970) and the phase. r_0 is estimated from a statistical sample of the seeing (von der Lühse 1984), on the order 100 frames. An atmospheric model then yields the long-exposure MTF, which is applied to an average of the Fourier amplitudes of the data frames. The estimation of the phases requires more effort, because the phases of the data frames average to zero. This is the same reason why a long-exposure image has very little phase information. However, there are differential quantities that do not average to zero. Two such quantities, introduced by Knox & Thompson (1974) and Weigelt (1977), are still the foundation of today’s SI codes, i.e., Knox–Thompson or speckle masking algorithms. Since low-contrast objects are common in solar imaging, special adaptations and improvements were invented by von der Lühse (1993), de Boer (1993), and Mikurda & von der Lühse (2006).

3.2 Multi-frame blind deconvolution

If an image is an unknown object convolved with an unknown PSF plus random noise, the blind deconvolution problem is to estimate both the unknown quantities. This problem is ill-posed, because an infinite number of PSF/object combinations can give a particular observed image. Therefore, we need constraints that make the correct solution more unique.

One powerful constraint is to require that the PSF can be directly related to the telescope's pupil and f -number in the presence of an unknown phase over the pupil. Other constraints are given by the use of multiple frames. A small number (~ 5) of frames is sufficient, although the results improve with the number of frames. The diversity of pupil phases facilitates the separation of PSFs and the common object. A special case is the introduction of a second detector, which simultaneously records defocused images. This PD technique (Gonsalves 1982) improves the identification of the aberrations in two ways: the defocus gives a known phase perturbation and the aberrations manifest themselves more clearly outside the focal plane, where the PSF wings are more pronounced.

The unknown phase is parameterized by expansion in a set of basis functions. An estimate of the expansion parameters is determined from iterative minimization of an error metric, which measures the difference between the observed images and synthetic images derived from estimated quantities (for some of the early development see, e.g., Ayers & Dainty 1988; Paxman et al. 1992; Schulz 1993).

Solar PD was independently developed by two teams (Löfdahl & Scharmer 1994a,b; Seldin & Paxman 1994), who used data from the Swedish Vacuum Solar Telescope (SVST) to establish PD as a reliable method for restoring solar data. A PD-restoration example is shown in Fig. 3. After Van Kampen & Paxman (1998) had demonstrated that solar MFBD is possible without PD, Löfdahl (2002) developed a more general formulation of the problem including PD. The new algorithm also accommodates simultaneously collected data at different wavelengths or with different polarization states. This Multi-Object MFBD (MOMFBD) approach was implemented by van Noort et al. (2005). The C++ code is publicly available from www.momfbd.org.

3.3 Issues common to SI and MFBD

Noise in solar images is mostly shot noise that comes from the quantum nature of light and an uncertainty in the number of electrons emitted by a photodetector. It is Poisson distributed but well approximated by additive Gaussian noise for large numbers of electron emissions. Low-pass filtering is routinely used to avoid noise amplification at high spatial frequencies. Observers, who want long-exposure images in order to improve the signal-to-noise ratio (SNR), should note that combining many short-exposure data frames gives the SNR corresponding to the total exposure time. There is also a fixed pattern component from pixel-to-pixel variations in detector element sensitivity and bias. This is easily corrected with standard flat-field pre-processing.

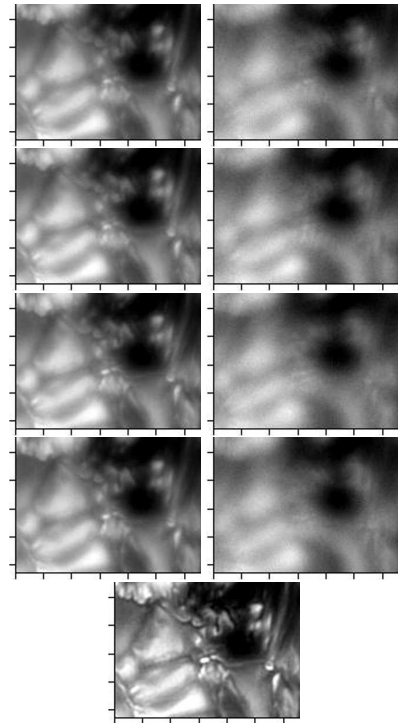


Figure 3. PD image restoration example. **Left:** in-focus images. **Right:** corresponding out-of-focus images. **Bottom:** restored object. Tickmarks: 1''.

The exposure time should be short enough so that the wavefront does not change significantly. The decorrelation time-scale of daytime seeing is ~ 50 ms, which sets the typical exposure time to ~ 10 ms for daytime observations. It also limits statistically independent samples to about 20 frames per second. On the other hand, the photospheric sound speed is 7 km/s or $0'.1$ /s as seen from Earth. At this speed, it takes only 5 s to cross half a $0'.1$ resolution element, which corresponds to the diffraction limit of a 1-m telescope. This leaves SI with just enough time to obtain the ~ 100 frames with an unchanging object, that are required for a good restoration. In the chromosphere, collection intervals should be even shorter, since the sound speed is several times larger than in the photosphere and magnetic forces can accelerate gas to even higher speeds, e.g., van Noort & Rouppe van der Voort (2006) observed optical flows in H α with speeds of up to 240 km/s.

PSFs are not space invariant, if extended scenes on the Sun are considered. Both SI and MFBD are performed on subfields with sizes corresponding to the isoplanatic patch. A mosaic of these subfields is then assembled to yield a restored image of the entire FOV. Simplified seeing models provide a rough estimate of the isoplanatic angle $\theta_0 = 0.314r_0/h$, where h is the distance to the seeing layer. Considering that θ_0 is only $1''$ for $h = 10$ km and $r_0 = 15$ cm, processing subfields a few times larger than this size surprisingly still produces satisfactory results.

The most demanding observing schemes now require several hundreds of image frames from different cameras per collection interval. While SI is non-iterative and scales linearly with the number of frames, MFBD is based on iterative, non-linear model-fitting, and scales badly with the number of frames. The difference is striking! In principle, $1k \times 1k$ pixel images can be SI restored on distributed computers in about the same time it takes to acquire the data (Denker et al. 2001). At the Dutch Open Telescope (DOT), e.g., a full day's observations are now SI restored in one night. In contrast, the Institute for Solar Physics assessed its need for computing resources. For the best possible MOMFBD restoration of 10 h worth of data (polarimeter in the red and Ca H scan in the blue, both with wide-band (WB) PD) from all cameras, a 100-CPU cluster would have to work for a full year.

3.4 Variants and new developments

Data collected through narrow-band (NB) filters in a dark spectral line have reduced SNR, which makes image restoration algorithms less effective. Keller & von der Lühe (1992) pioneered a technique called speckle deconvolution, using simultaneous frames collected with a WB continuum filter with better SNR. The object estimate from SI processing of the WB data together with the original frames yield the PSFs needed to deconvolve the NB data. This technique is now widely used for spectroscopy and polarimetry (see, e.g., Koschinsky et al. 2001).

While a similar scheme is possible for MFBD methods, the model fitting approach is facilitated by co-processing of WB and NB data, in order to use the available information as efficiently as possible. This MOMFBD method is illustrated in Fig. 4. The setup contains a NB camera behind the SOUP birefringent filter and two WB cameras in a PD configuration. Further, because the SOUP is not equipped with a polarizing beamsplitter, images at different polarization states have to be collected consecutively rather than in parallel. Anisoplanatic

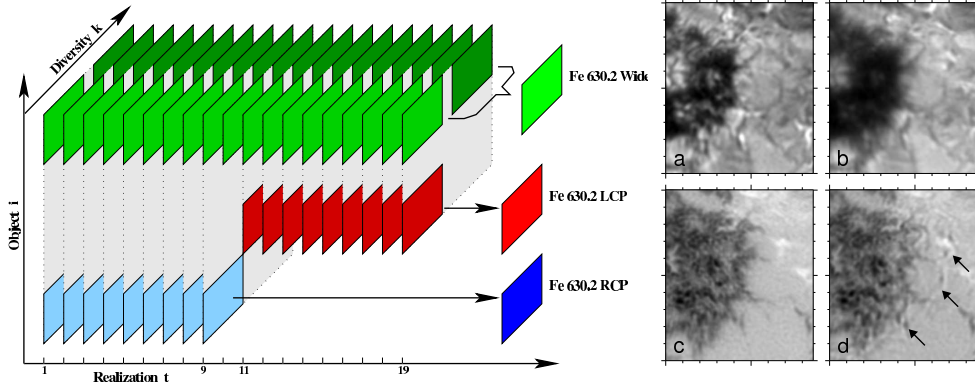


Figure 4. MOMFBD. **Left:** Graphic representation of constraints for a WB PD plus NB polarimetry setup. Simultaneous wavefront coefficients are required to be identical. As a consequence, the NB restorations are aligned with the WB restoration and therefore to each other. **Right:** (a) and (b) show restored Fe 630.2 nm (-6 pm from the core) right- and left-hand circularly polarized (RCP and LCP) images, respectively. (c) and (d) show line-of-sight (LOS) magnetograms made by subtracting the RCP and LCP images. In (c) the alignment is calibrated as part of the MOMFBD procedure. In (d) the alignment is based on sub-image cross-correlation and destretching. Arrows indicate artifacts from seeing-related alignment mismatches. Tickmarks: $1''$ (Adapted from van Noort et al. (2005)).

seeing during the collection interval makes such images imperfectly aligned, a problem that can be calibrated using a pinhole array as target. The problem is constrained by the fact that the wavefronts corresponding to the simultaneously recorded images have to be the same. Because each raw NB frame is simultaneously taken with a PD pair, both restored NB images will be aligned to the WB restoration and thus to each other. The restored NB images can then produce magnetograms without further alignment or destretching – a procedure that is prone to producing seeing-related artifacts because it involves cross-correlation of nonidentical images.

SI AO. SI can well estimate the Fourier phases of AO-corrected solar images (Denker et al. 2005). However, the restored power spectrum is not correctly estimated because of how AO correction modifies the statistics of the atmospheric aberrations. Puschmann & Sailer (2006) included AO modeling in their speckle masking code (see Fig. 5). They demonstrate that traditional SI, with a single r_0 , over-corrects near the AO sensor lockpoint, while allowing for a varying r_0 over-corrects with distance from the lockpoint. Including modeling of the AO correction is better in the sense that the restored “quiet sun” contrast varies less with lockpoint distance. While this appears to be a valid approach to the problem, work still remains to be done before it is a mature solution. The Swedish Solar Telescope (SST) data shown in Fig. 5 were collected when the AO was locking during almost the entire collection interval. Processing a data set with AO lock only part of the time requires logging of the AO performance as well as more modeling work.

SI . While data from a slit-spectrograph is one-dimensional, one can get two-dimensional information by scanning with the slit. The result is a data cube, which is unfortunately not only blurred by the seeing but also irregularly sampled due to anisoplanatic distortions. Keller & Johannesson (1995) implemented a method where the cube is

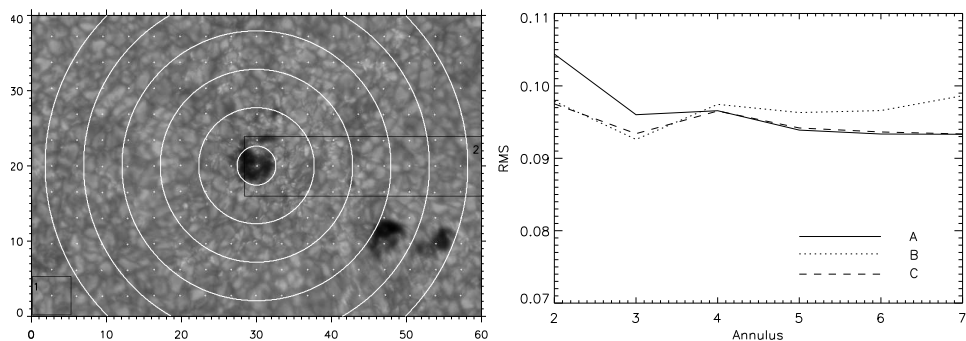


Figure 5. SI with AO correction. Restorations using three different methods: *A*: traditional, *B*: using a spatially varying r_0 , and *C*: with AO modeling. **Left:** Raw image with annuli centered on the pore, which was used as the AO wavefront sensor target. **Right:** Restored contrast in the different annuli (with magnetic structures removed) for the three different methods demonstrating that model *C* produces the flattest contrast profile. Tickmarks: $1''$ (Adapted from Puschmann & Sailer (2006)).

resampled so that the continuum is aligned to an SI restoration of the slit-jaw images. The cube is also deconvolved using information from the slit-jaw SI processing.

4 Discussion

Image restoration is needed to fully utilize the resolution of modern solar telescopes. AO will always leave uncorrected residuals, particularly away from the wavefront sensor FOV. There are two kinds of methods in routine use: SI and MFBF methods. Both are actively used for producing science data and both are still being developed in order to meet demands and challenges from new observations and instruments. Still, the differences between the methods give them different strengths and weaknesses.

SI does not have strict requirements for the optical setup, other than a camera fast enough to collect a statistical sample in a short time. This can lead to very large data amounts (TBytes) over an observing day. In addition, it may be difficult to collect sufficient independent samples for a quickly evolving target without violating the assumption of an unchanging object. On the other hand, SI is more robust for low contrast data than MFBF methods, which are more dependent on finding structures in the data.

In its simplest form, MFBF does also not require any extra optics and has the advantage that the sample does not have to be as large. MFBF processing is the best thing that can be done, if less images are available than required for a statistical sample. However, the number of frames needed for NB data primarily depends on SNR requirements. In addition, the inclusion of PD requires an extra camera or extra optics.

The greatest drawback of MFBF methods is the computing time. A full day's worth of DOT data can be SI restored overnight, while one day of SST data may require almost an entire year for full MOMFBF processing. While this may become less of a problem as the cost for CPU cycles continues to decrease, the choice now clearly has to be guided by whether we need high-volume, routine restoration or are aiming for a few unique data sets.

MFBF makes no assumption about seeing characteristics. This means there are no prob-

lems with fixed aberrations or time- and space-varying AO corrections. On the other hand, MFBF restorations systematically under-estimate power spectra due to the finite expansion of the wavefronts. If the underlying atmospheric model is correct, SI should automatically obtain the correct power spectra. However, AO-corrected data are not as easily modeled, although method development is making rapid progress to address this problem.

Acknowledgements. This work was supported in part by NSF under grants IIS ITR 03-24816 (ML and CD) and ATM 02-36945 (CD). The Swedish 1-m Solar Telescope is operated by the Institute for Solar Physics of the Royal Swedish Academy of Sciences on the island of La Palma at the Spanish Observatorio del Roque de los Muchachos of the Instituto de Astrofísica de Canarias.

References

- Ayers, G. R. & Dainty, J. C. 1988, *Opt. Lett.*, 13, 547
 Berkefeld, T. 2007, (this volume)
 de Boer, C. R. 1993, PhD thesis, University of Göttingen
 Denker, C., Mascariñas, D., Xu, Y., et al. 2005, *Solar Phys.* 227, 217
 Denker, C., Yang, G., & Wang, H. 2001, *Solar Phys.* 202, 63
 Fried, D. L. 1966, *J. Opt. Soc. Amer.* 54, 1372
 Gonsalves, R. A. 1982, *Opt. Eng.*, 21, 829
 Keller, C. U. & Johannesson, A. 1995, *A&A Suppl.* 110, 565
 Keller, C. U. & von der Lühse, O. 1992, *A&A* 261, 321
 Knox, K. T. & Thompson, B. J. 1974, *ApJ* 193, L45
 Koschinsky, M., Kneer, F., & Hirzberger, J. 2001, *A&A* 365, 588
 Labeyrie, A. 1970, *A&A* 6, 85
 Löfdahl, M. G. 2002, in: *Proc. SPIE* 4792, 146–155
 Löfdahl, M. G. & Scharmer, G. B. 1994a, in: *Proc. SPIE* 2302, 254–267
 Löfdahl, M. G. & Scharmer, G. B. 1994b, *A&A Suppl.* 107, 243
 Mikurda, K. & von der Lühse, O. 2006, *Solar Phys.* 235, 31
 Paxman, R. G., Schulz, T. J., & Fienup, J. R. 1992, *J. Opt. Soc. Amer. A* 9, 1072
 Puschmann, K. G. & Sailer, M. 2006, *A&A* 454, 1011
 Rimmele, T. R. 2000, in: *Proc. SPIE* 4007, 218–231
 Roddier, F. 1981, in: *Progress in Optics* 19, ed. E. Wolf (Amsterdam: North-Holland Publishing Company), 281–376
 Scharmer, G. B., Shand, M., Löfdahl, M. G., Dettori, P. M., & Wei, W. 2000, in: *Proc. SPIE* 4007, 239–250
 Schulz, T. J. 1993, *J. Opt. Soc. Amer. A* 10, 1064
 Seldin, J. H. & Paxman, R. G. 1994, in: *Proc. SPIE* 2302, 268–280
 Stevens, E. G. & Lavine, J. P. 1994, *IEEE transactions on electronic devices*, 41, 1753
 Van Kampen, W. C. & Paxman, R. G. 1998, in: *Proc. SPIE*, Vol. 3433, *Propagation and Imaging through the Atmosphere II*, ed. L. R. Bissonnette, 296–307
 van Noort, M., Rouppe van der Voort, L., & Löfdahl, M. G. 2005, *Solar Phys.* 228, 191
 van Noort, M. J. & Rouppe van der Voort, L. H. M. 2006, *ApJ* 648, L67
 von der Lühse, O. 1984, *J. Opt. Soc. Amer. A* 1, 510
 von der Lühse, O. 1993, *A&A* 268, 374
 Weigelt, G. P. 1977, *Optics Communications*, 21, 55